Fibroblast Growth Factor Receptor 3 activation plays a causative role in urothelial cancer pathogenesis in cooperation with *Pten* loss in mice

Mona Foth[1, 2], Imran Ahmad[2], Bas W. G. van Rhijn[3], Theodorus van der Kwast[4], Andre M. Bergman[4], Louise King[1], Rachel Ridgway[2], Hing Y. Leung[2], Sioban Fraser[5], Owen J. Sansom[2] and Tomoko Iwata[1*]

[1]School of Medicine, College of Medical, Veterinary and Life Sciences, University of Glasgow, [2]Beatson Institute for Cancer Research, Glasgow, United Kingdom, [3]Division of Surgical Oncology (Urology), Netherlands Cancer Institute – Antoni van Leeuwenhoek Hospital, Amsterdam, The Netherlands, [4]Department of Pathology, University Health Network, Princess Margaret Hospital, Toronto, Canada, [5]Department of Pathology, Southern General Hospital, Glasgow, United Kingdom

*Correspondence

School of Medicine, College of Medical, Veterinary and Life Sciences, University of Glasgow, University Pathology, Southern General Hospital, 1345 Govan Road, Glasgow, G51 4TF, United Kingdom

Tel; +44 141 354 9438

Fax; +44 141 232 7991

Email; Tomoko.Iwata@glasgow.ac.uk

No conflicts of interest were declared.

This article has been accepted for publication and undergone full peer review but has not been through the copyediting, typesetting, pagination and proofreading process, which may lead to differences between this version and the Version of Record. Please cite this article as doi: 10.1002/path.4334

Abstract

Although somatic mutations and overexpression of the tyrosine kinase *Fibroblast Growth Factor Receptor 3* (*FGFR3*) are strongly associated with bladder cancer, evidence for their functional involvement in the pathogenesis remains elusive. Previously we showed that activation of Fgfr3 alone is not sufficient to initiate urothelial tumourigenesis in mice. Here we hypothesise that cooperating mutations are required for Fgfr3-dependent tumourigenesis in the urothelium and analyse a mouse model in which an inhibitor of Pi3k-Akt signalling, *Pten*, is deleted in concert with Fgfr3 activation (*UroIICreFgfr3*$^{+/K644E}$*Pten*$^{flox/flox}$). Two main phonotypical characteristics observed in the urothelium were increased urothelial thickness and abnormal cellular histopathology, including vacuolisation, condensed cellular appearance, enlargement of cells and nuclei, and loss of polarity. These changes were not observed when either mutation was present individually. Expression patterns of known urothelial proteins indicated the abnormal cellular differentiation. Furthermore, quantitative analysis showed that *Fgfr3* and *Pten* mutations cooperatively caused cellular enlargement, while *Pten* contributed to an increased cell proliferation. Finally, FGFR3 overexpression was analysed along the level of phosphorylated mTOR in sixty-six T1 urothelial tumours in tissue microarray, which supported the occurrence of functional association of these two signalling pathways in urothelial pathogenesis. Taken together, this study provides evidence supporting a functional role of FGFR3 in the process of pathogenesis in urothelial neoplasm. Given the wide availability of inhibitors specific to FGF signalling pathways, our model may open the avenue for FGFR3-targeted translation in urothelial disease.

Keywords: transitional cell carcinoma, transgenic mouse model, Fibroblast Growth Factors, prognostic marker, personalised therapy, comparative pathology

Introduction

The majority of bladder cancers are urothelial carcinomas (UC) that occur in the urothelial lining and present as either non-muscle invasive (NMIBC) or muscle-invasive bladder cancers (MIBC). Clinically operable MIBC are treated with radical cystectomy or radiotherapy, however up to 50% of the patients relapse [1]. NMIBC tends to recur frequently and it is estimated that 10-20% of NMIBC potentially progress MIBC [2,3]. A number of genetic and epigenetic alterations have been identified in MIBC, including amplification of *ERBB2* and loss of *TP53, Retinoblastoma* (*RB*) and the *phosphatase and tensin homolog* (*PTEN*) [4]. NMIBC is strongly associated with activating mutations in *FGFR3* with a frequency between 60-80% [5-8], followed by chromosome 9 deletion (36-66%) and mutations in *RAS* family genes and in *Phosphatidylinositol-4,5-Bisphosphate 3-Kinase Catalytic Subunit Alpha* (*PIK3CA*) [4]. FGFR3 protein is also overexpressed in 42% of bladder tumours without FGFR3 mutations [49].

FGFR3 is a tyrosine kinase receptor that mediates the effects of Fibroblast Growth Factors (FGFs) [9]. FGFR3 mainly stimulates the RAS-Mitogen-Activated Protein Kinase (MAPK) and Phosphatidylinositide-3 Kinase (PI3K)-AKT pathway and triggers a range of cellular processes such as cell proliferation and differentiation. When activating mutations occur in the germ line, FGFR3 causes several forms of dwarfism: hypochondroplasia, achondroplasia and thanatophoric dysplasia, and malformation of the cerebral cortex [10-13]. *FGFR3* mutations are identified also in several cancer types, including multiple myeloma, cervical, prostate cancer and spermatocytic seminomas [14]. The functional role of *FGFR3* mutation in tumour formation was first demonstrated in multiple myeloma [15], skin hyperplasia in transgenic mice overexpressing mutant *FGFR3* [16] and in xenograft models [17]. However

the mechanistic role of *FGFR3* activation caused by mutations and overexpression in bladder tumourigenesis remains to be elucidated.

We have previously used a mouse line in which *K644E,* a highly activating mutation in the *Fgfr3* kinase domain, is conditionally expressed in the urothelium (*UroIICreFgfr3*$^{+/K644E}$) to investigate the functional role of Fgfr3 activation in bladder tumourigenesis [18]. These mice did not show any urothelial phenotype, indicating that Fgfr3 activation alone is not sufficient to drive tumourigenesis in the urothelium. However, in combination with *K-Ras* or *β-Catenin,* Fgfr3 activation caused tumours in the skin and in the lungs, respectively, suggesting that Fgfr3 is able to induce tumourigenesis in the presence of cooperating mutations [18]. We found that the Pi3k-Akt pathway was highly up-regulated in lung tumours which formed in the presence of *Fgfr3* and *β-Catenin* mutations, while in the urothelium this up-regulation was not observed. This has led us to hypothesise that urothelial tumourigenesis may require increased PI3K-AKT signalling. In humans, activating *PIK3CA* mutations, including those at the hotspots (E542K, E545K in the helical domain and H1047R in the kinase domain), are found in 13-25% of bladder cancer [31,41-45]. Interestingly, *FGFR3* and *PIK3CA* mutations are shown to co-occur [31,41-45]. Therefore it was proposed that activation of PI3K-AKT pathway may enhance the effects of *FGFR3* mutation [30,31].

In this study, we wished to test the synergistic effects of *Fgfr3* and Pi3k-Akt signalling activation. PTEN is a well-known inhibitor of PI3K-AKT signalling and previous mouse models demonstrated that the loss of *Pten* leads to urothelial hyperplasia [19,20]. Therefore we used the mouse line with *Pten* deletion as an experimental tool to assess the effects of Pi3k-Akt activation in the presence of *Fgfr3* mutation in the urothelium. The urothelium of double mutant mice was thickened and showed abnormal cellular features including enlarged

cells and loss of polarity. The mechanisms leading to this phenotype was further investigated for cell differentiation, cell proliferation and apoptosis. Finally, the synergistic effects of mutations in downstream signalling were characterised in the mouse urothelium, and evaluated along the level of FGFR3 overexpression in clinical specimens in the tissue microarray (TMA) platform.

Materials and Methods

Mice: *UroIICre* transgenic mice [23] were intercrossed with *Fgfr3*$^{+/K644Eneo}$ [11] and *Pten*$^{flox/flox}$ mice [24] to generate *UroIICreFgfr3*$^{+/K644E}$*Pten*$^{flox/flox}$. Except for *UroIICre* (FVB/N), background of mice was C57Bl/6. The Z/EG reporter line is from Novak et al., 2000 [25]. Genotype was performed by Transnetyx, USA. The *Control* were C57Bl/6 (n=7) (Charles River, UK) and mice that carries inactive *'T2/Onc3'* transposon allele [26] (n=4) which do not lead to any phenotype. All experiments were carried out in accordance with the Project Licence under Home Office Animal (Scientific Procedures) Act 1986 in the UK.

Histology: Bladders were gently emptied of urine and placed in formalin for overnight fixation. Haematoxylin and eosin (H&E) and PAS staining (Leica Microsystems staining solutions #3803812 and #03800E) was performed on 4 μm-thick paraffin sections. Formalin-fixed OCT-embedded frozen sections were used in X-Gal staining (K1465-01, Invitrogen Life Technologies, UK).

Immunohistochemistry (IHC): Antigen retrieval was performed with 0.01M citric acid (pH 6) unless specified otherwise. Samples were incubated in 0.3% H_2O_2 in distilled water for 20 min. Following the blocking, incubation with primary antibody was performed overnight at

4ºC, with secondary antibody for 2 hours at room temperature. Antibody binding was visualised by ABC Elite Standard kit (Vector Labs, PK-6100) and 3,3'-Diaminobenzidine (DAB; K3468, Dako), counterstained with haematoxylin. For fluorescent visualisation, sections were incubated with 4',6-diamidino-2-phenylindole (DAPI; 1:1000) and mounted with Vectashield (Vector Labs, H-1000). Pictures were taken by Axio Imager (Zeiss A1) and Zeiss upright confocal microscope (Zeiss 710) for light and fluorescent microscopy, respectively. The slides were scanned by Nanozoomer slide scanner (Hamamastu) and analysed by SlidePath Digital Image Hub (Leica Biosystems). IHC staining was examined in the minimum of n=3 per genotype. Antibodies used were: Caspase-3 (R&D Systems, AF835; 1:200), CK5 (Abcam, ab24647, 1:500), CK18 (Progen, #61028, 1:10), GFP (Abgent, AM1009a; 1:25), E-cadherin (BD Transduction Laboratories Clone 36; 1:1000), pERK1/2 (Cell Signaling, #9101 and #4370; 1:100), FGFR3 (Santa Cruz Biotechnology, C-15; 1:40, no antigen retrieval), Ki67 (Vector Labs Burlingame USA, VP-RM04; 1:100), Pten (Cell Signaling, #9559; 1:100), UroII (Santa Cruz, #sc15178, 1:50), pAkt1/2 (Ser473) (Cell Signalling, #3787; 1:50), p21 (Santa Cruz, M19; 1:500), p63 (Santa Cruz, sc-8431, 1:100). Biotinylated goat secondary antibodies from Vector Labs, Anti-Rabbit IgG (BA-1000), Anti-Rat IgG (BA-9401), and Anti-Mouse IgG (BA-9200) were used for chromatogenic signals, Alexa Fluor 488 Goat Anti-Mouse IgG_1 (Invitrogen, A-21121) and Alexa Fluor 594 Goat Anti-Rabbit IgG (Invitrogen, A-11012) were used for fluorescent.

Quantitative analysis; Three representative photos were taken for each H&E stained section at 40x magnification. Urothelial thickness was measured in 25-30 µm intervals at random fashion using ImageJ software (NIH, Bethesda, USA). Each picture contained 20-50 measurements. The mean value of the thickness was initially calculated for each sample, and subsequently the mean value in each genotype was determined as presented in the results. For

cell size, each cell was marked around the cell membrane in E-cadherin stained sections and the areas were quantified using ImageJ. The sizes of fifteen cells each layer were measured per sample. For quantitative analysis, the umbrella layer was defined as the outermost single layer, basal layer the innermost, and the intermediate cell layer between those two in the urothelium. Cells positive with Ki67 or Caspase-3 staining, as well as total cell number in the urothelium were counted. The percentage of Ki67 or Caspase-3-positive cells within the total cell number was calculated per sample and the mean value was determined in each genotype. Statistics were performed using the Mann-Whitney test for non-parametric distribution of data (SPSS Version 19, IBM).

Tissue microarray (TMA) analysis of clinical specimens: With the ethical approval under the medical-ethical committee of the University Health Network, Toronto, T1 urothelial tumours on TMA were stained with FGFR3 (Santa Cruz, B-9; 1:300, overnight incubation) and p-mTOR(S2448) (Cell Signaling, #2976; 1:30). Positive and negative controls were included in each run. Slides were assessed by the pathologists. Both protein levels were scored based on membrane staining according to the 4-point scale (0=negative, 1=faint, 2=intermediate, 3=strong) (Figure S5). Correlation was statistically evaluated by Pearson Chi-square statistics (SPSS).

Results

Together with *Pten* loss, the activating *Fgfr3* mutation increases the thickness of the urothelium in mice.

In order to see whether Fgfr3 activation is able to form UC in the absence of *Pten*, we generated a cohort of *UroIICreFgfr3*$^{+/K644E}$*Pten*$^{flox/flox}$ mice. In these mice, the heterozygous

Fgfr3 K644E knock-in mutation [11] and deletion of both *Pten* alleles [24] occurs concomitantly in the urothelium [27]. Cohorts of *UroIICreFgfr3*$^{+/K644E}$, *UroIICrePten*$^{flox/flox}$ and *UroIICreFgfr3*$^{+/K644E}$*Pten*$^{flox/flox}$ were examined at 5-18 months (Table 1). Cre-dependent recombination in the urothelium was assessed using *Z/EG* reporter mice. In the presence of the *UroIICre* allele, cells with a GFP-positive nucleus were observed in the majority of urothelial cells (Figure S1h) while little X-gal staining remained in the urothelium (Figure S1i), confirming successful recombination. We detected similar levels and patterns of Fgfr3 protein expression in the urothelium of *Control* and *UroIICreFgfr3*$^{+/K644E}$ (Figure S1a, b) as we reported previously [18], and in *UroIICrePten*$^{flox/flox}$ and *UroIICreFgfr3*$^{+/K644E}$*Pten*$^{flox/flox}$ (Figure S1c, d), indicating that Fgfr3 expression was neither influenced by the *Fgfr3* mutation nor *Pten* deletion. An increased FGFR3 protein level observed in 85% of bladder tumours with *FGFR3* mutations in humans [49] was not apparent. Lack of Pten expression was confirmed in *UroIICrePten*$^{flox/flox}$ urothelium (Figure S1g). Levels of Pten protein were similarly low in *Control* and *UroIICreFgfr3*$^{+/K644E}$ (Figure S1e, f), indicating that Pten expression is unaltered in the presence of *Fgfr3* mutation.

We observed a severe increase in thickness of the urothelium in *UroIICreFgfr3*$^{+/K644E}$*Pten*$^{flox/flox}$ mice compared to *Control* (Table 1, Figure 1). A mild increase was also observed in 60% of *UroIICrePten*$^{flox/flox}$, while the thickness of *UroIICreFgfr3*$^{+/K644E}$ urothelium was normal. The urothelium of mice with homozygous *Fgfr3* mutation (*UroIICreFgfr3*$^{K644E/K644E}$) showed a mild thickening (Table 1, Figure S1k, l). In contrast, mice with homozygous mutations in both *Fgfr3* and *Pten* (*UroIICreFgfr3*$^{K644E/K644E}$*Pten*$^{flox/flox}$) revealed a similar phenotype to that of *UroIICreFgfr3*$^{+/K644E}$*Pten*$^{flox/flox}$ (Figure S1m, n).

We have quantified these changes in mice aged between 11-18 months. Consistent with our previous observations [18,21], urothelial thickness of *UroIICreFgfr3*$^{+/K644E}$ and *UroIICrePten*$^{flox/flox}$ were similar to *Control* (Figure 1i). However, thickness was significantly increased when both mutations were present in *UroIICreFgfr3*$^{+/K644E}$*Pten*$^{flox/flox}$ compared to either *UroIICreFgfr3*$^{+/K644E}$ (p=0.00005) or *UroIICrePten*$^{flox/flox}$ (p=0.00049), suggesting that this increase is generated by the cooperation of *Fgfr3* and *Pten* mutations.

Abnormal histopathology of the *UroIICreFgfr3*$^{+/K644E}$*Pten*$^{flox/flox}$ urothelium

In addition to increased urothelial thickness, several abnormal cellular morphologies were observed in *UroIICreFgfr3*$^{+/K644E}$*Pten*$^{flox/flox}$, including vacuolisation, condensed cellular appearance, enlargement of cells and nuclei, and loss of polarity (Figure 2A). High glycogen levels were detected in vacuoles by Periodic acid-Schiff (PAS) staining (n=3) (Figure 2Ag). At least one of these cellular features were observed in the majority of *UroIICreFgfr3*$^{+/K644E}$*Pten*$^{flox/flox}$ (83%), while none of these abnormal features were present in *Control* (Figure 2Aa, d), *UroIICreFgfr3*$^{+/K644E}$ or *UroIICrePten*$^{flox/flox}$ urothelium (Table 1).

In order to see whether these abnormal cellular appearances are caused by a change in urothelial cell identities, staining was performed with urothelial markers well-established in mice, UroII (umbrella and some intermediate cells [28]), Cytokeratin 5 (CK5) (basal cells [29]) and p63 (basal and intermediate cells [30]) (Figure 2Ba-c). In *UroIICreFgfr3*$^{+/K644E}$*Pten*$^{flox/flox}$, UroII-positive cells were present in deeper layers close to the submucosa, while CK5 expression was absent in some parts of the innermost layers of the urothelium, showing an inverse expression pattern (Figure 2Be, f, i, j). Furthermore, p63 showed a disorganised expression pattern (Figure 2Bg, k). Double staining of CK18, an alternative marker of umbrella cells in mice [30], together with CK5 clearly showed the

abnormal localisation of CK18-positive cells deep in the urothelium of *UroIICreFgfr3*$^{+/K644E}$*Pten*$^{flox/flox}$ (Figure 2Bh, l). Taken together, the results indicated abnormal differentiation of urothelial cells in *UroIICreFgfr3*$^{+/K644E}$*Pten*$^{flox/flox}$.

Urothelial cell size and proliferation is differently regulated by *Fgfr3* and *Pten* mutations

The increase in urothelial thickness can be caused by deregulation of cell size and/or cell number. No significant difference in cell size was observed in the innermost basal and outermost umbrella layers among the cohorts (Figure 3a, c). In contrast, in the intermediate (between the inner and outermost) urothelial layers, while *Fgfr3* mutation alone did not influence the cell size, *Pten* loss alone increased the cell size compared to *Control* (p=0.017) (Figure 3b). Furthermore, the presence of both *Fgfr3* and *Pten* mutations further increased the cell size comparing to *Fgfr3* mutation alone (p=0.001), as well as to *Pten* alone (p=0.016), suggesting that the *Fgfr3* mutation cooperates with the *Pten* loss to further increase the cell size.

Albeit in a relatively small number of cells, Ki67 positivity was identified in all layers of the urothelium, including umbrella cells (Figure S2a, b) [30]. Taken all layers together, a significant increase in Ki67-positive cells was seen in the presence of both *Fgfr3* and *Pten* mutations (p=0.004), as well as in the presence of *Pten* loss only (p=0.009), compared to *Fgfr3* mutation only (Figure 3d). This indicates that cell proliferation was increased due to *Pten* loss. Similar effects were observed in the outermost and intermediate layers, while no significant changes were seen in the innermost basal layer (Figure S2). Very few apoptotic events were observed in all cohorts (Figure S3).

In summary, these results indicate that *Fgfr3* and *Pten* mutations cooperatively caused urothelial hypertrophy, while *Pten* contributed to hyperplasia in the *UroIICreFgfr3*$^{+/K644E}$*Pten*$^{flox/flox}$ urothelium.

Changes in downstream signalling associates with abnormal differentiation

We addressed how *Fgfr3* and *Pten* mutations altered their downstream signalling cascades using antibodies for the phosphorylated forms of Erk1/2 (pErk1/2) and Akt(Ser473) (pAkt). In *Controls,* pErk1/2 was observed in a patchy fashion in the urothelium, not limited to a particular cell or cell type (n=9) (Figure 4a). Staining was similar in *UroIICreFgfr3*$^{+/K644E}$ (n=9) and *UroIICrePten*$^{flox/flox}$ (n=6/9) (Figure 4d, g). In contrast, in *UroIICreFgfr3*$^{+/K644E}$*Pten*$^{flox/flox}$ samples (n=9/12, 75%) pErk1/2 was seen more in a cell-specific fashion (Figure 4j), which resembled the overall pattern of UroII and CK5 staining (Figure 2B). As this staining was rather unusual, an alternative pErk antibody was also used to confirm this pattern (Figure S4). This observation may suggest the involvement of local MapK signalling dysregulation in pathogenesis of the urothelium through regulation of cell differentiation. However this requires further investigation. The staining of pAkt was absent in *Control* (n=3), *UroIICreFgfr3*$^{+/K644E}$ (n=6) and *UroIICrePten*$^{flox/flox}$ (n=7) (Figure 4b, e, h), but found to be up-regulated in 55% of *UroIICreFgfr3*$^{+/K644E}$*Pten*$^{flox/flox}$ samples (n=6/11, Figure 4k). Cyclin-dependent kinase inhibitor and tumour suppressor p21 was previously shown to be up-regulated in the mouse urothelium in which *Pten* is deleted [20]. p21 was present most abundantly in the outermost umbrella layer in *Control* (n=3) (Figure 4c), and this remained similar in *UroIICreFgfr3*$^{+/K644E}$ (n=3) and *UroIICrePten*$^{flox/flox}$ (n=3) in this study (Figure 4f, i). However, in *UroIICreFgfr3*$^{+/K644E}$*Pten*$^{flox/flox}$ urothelium (n=4), p21 was expressed throughout the urothelium (Figure 4l). This p21 up-regulation appeared to have coincided with the overall up-regulation of Pi3k-Akt signalling (Figure 4k), which is in

accordance with the evidence *in vitro* that activation of PI3K-AKT pathway up-regulates p21 [48]. Altogether, these results provide the evidence to support the activation of Pi3k-Akt pathway in the current mouse model, as a result of cooperation between *Fgfr3* and *Pten* mutations together, but not when either mutation was present individually.

Previous studies have investigated mutations in *FGFR3* and PI3K-AKT pathway genes [31, 41-47] and their activation, using antibodies specific to the phosphorylated form of the protein, such as pAKT [43-45,47]. Mammalian Target of Rapamycin (mTOR) is downstream of PI3K-AKT signalling, and a candidate for effective therapeutic target [21,22]. We evaluated the levels of FGFR3 protein and p-mTOR(S2448) in 66 T1 urothelial tumours in TMA (Figure 4m, Figure S5). While the decrease in strong FGFR3 was statistically not significant (p=0.101), an increase in intermediate FGFR3 expression was correlated with an increased level of p-mTOR (p=0.014), supporting the presence of functional synergy of FGFR3 and PI3K-AKT pathways.

Discussion

FGFR3 mutations are highly associated with NMIBC [5,32]. A series of studies have shown the frequent co-occurrences of *FGFR3* and *PIK3CA* mutations and evaluated gene alterations in PI3K-AKT pathway in clinical cohorts of bladder cancer [31,41-47]. However functional cooperation between Fgfr3 and Pi3k-Akt activation has never been demonstrated before. As both mutations and overexpression of FGFR3 is also highly associated with bladder cancer [49], our approach was to address the role of Fgfr3 activation using the existing mouse line with *Fgfr3 K644E* mutation [11,18]. Although the kinase domain mutations are less common

in contrast to *S249C* in humans [5,32], this mouse line offers several advantages as an experimental model, namely because the Cre-Lox construct enables the expression of mutant *Fgfr3* in the urothelium-specific fashion and the mutation is highly activating, thus maximising the chance of detectable phenotype. In the absence of available mouse lines with *PI3KCA* mutations, we turned to a model that enables conditional *Pten* deletion [19,20]. Pten is a well-known inhibitor of Pi3k-Akt signalling and it was shown that its deletion resulted in pAkt up-regulation in bladder tumours in mice [21].

Significantly, while the papillary structures with fibro-vascular cores seen in human NMIBC were not observed, the urothelium of *UroIICreFgfr3*$^{+/K644E}$*Pten*$^{flox/flox}$ did demonstrate several morphological abnormalities that may reflect pathogenesis in humans. Two main phenotypes were increased urothelial thickness (Figure 1) and abnormal urothelial cellular histopathology, including vacuolisation, condensed cellular appearance, enlargement of cells and nuclei, and loss of polarity (Figure 2). *Fgfr3* and *Pten* mutations cooperatively caused urothelial hypertrophy through regulation of cell size, while increased cell proliferation was mainly an effect of *Pten* deletion (Figure 3). The pErk staining in the double mutant urothelium showed an unusual cell-specific pattern (Figure 4j) and may suggest the local involvement of MapK pathway in pathogenesis through regulation of cell differentiation. These histopathological features are comparable to hyperplasia and dysplasia, regarded as early stages in the putative model of bladder cancer pathogenesis in humans. To our knowledge, this is a unique observation that has not been reported in any other genetic models of urothelial abnormalities.

Furthermore, up-regulation of pAkt was observed when both *Fgfr3* and *Pten* mutations together, and not in single mutants (Figure 4). In humans, higher pAKT level was found in

50% bladder tumours independent of stage/grades and is associated with the presence of mutations, including *PIK3CA, FGFR3,* and both together [43]. Activation of PI3K-AKT downstream protein, mTOR, is confirmed to be strongly associated with pAKT [47]. Relationship between FGFR3 overexpression and p-mTOR is relatively unstudied and one report showed no statistical association [47]. However, in the current study, although the number of samples analysed was small, we were able to show association of the intermediate level of FGFR3 overexpression with increased p-mTOR (Figure 4m). In humans, *PIK3CA* mutations were also found in normal urothelium, indicating that it is an early event [44]. Altogether, this study provide functional evidence that supports that up-regulation of FGFR3 signalling together with that of PI3K-AKT signalling plays a role in the initiation of urothelial tumourigenesis.

In contrast, the current model with *Fgfr3* and *Pten* mutations did not produce tumours in the life time of the animal models up to 18 months. This indicates that pathogenesis caused by *FGFR3* and PI3K-AKT signalling pathway mutations are unlikely to progress unless further mutations occur. Our data in mice show that *Fgfr3* and *Pten* mutations cooperatively promote morphological changes of the urothelium, while not when mutated individually. Previously it was reported that loss of *Pten* alone leads to urothelial hyperplasia [19,20]. However, hyperplasia was not observed by *Pten* loss in the studies by our group [21] and others [22]. In the current study, although mild urothelial thickening was observed in 60% of the *UroIICrePten*$^{flox/flox}$ mice (Table 1), this increase was statistically not significant upon quantification (Figure 1i). An *in vitro* study using Normal Human Urothelial Cells stably expressing the hotspot *PI3KCA* mutations showed a large, vacuolated and flattened morphology [33]. Cell proliferation was also increased in cells with helical domain mutant. Despite the difference that these effects were singly resulted by PIK3CA activation *in vitro*,

the findings are supportive of our observations in mice. This may reflect the complexity of signalling events leading to tumourigenesis *in vivo* in which multiple gene mutations and epigenetic events are likely to be required.

There are several differences between the natures of our mouse model in relationship to human bladder cancer that may limit the direct interpretation. Firstly, although we used *Pten* loss as an experimental tool in this study, in humans, occurrence of *FGFR3* mutations are associated with NMIBC while *PTEN* loss with MIBC, and therefore little overlap is expected [4,41]. *FGFR3* mutations and loss of heterozygosity in *PTEN* are found together only in a small number of cases of TaG1, T1G2, and T2G3 (Table S5 in ([41]). Statistically, *PTEN* loss was not associated with up-regulation of pAKT in clinical bladder cancer specimens [46]. Secondly, a study of clinical specimens reported that 85% of tumours with *FGFR3* mutations also overexpressed FGFR3 protein [49]. In contrast, changes in Fgfr3 protein level were not apparent in our model (Figure S1a-d). This could be due to the expected low level of endogenous protein expressed in the mouse urothelium. The mechanism of *FGFR3* mutations leading to an increased protein level is unclear, however the *in vitro* studies showed that impaired lysosomal degradation of FGFR3 protein was caused by mutations, increasing the stability of FGFR3 mutant protein in the plasma membrane [40].

FGF signalling inhibitors have been developed and applied in many cancer types [34]. Inhibition of FGFR had been suggested as a therapeutic option of UC [35]. Several novel drugs against FGFRs, including R3Mab [17], BGJ398 [36] and AZD4547 [37], are shown to be effective in cell lines and xenograft models. A recent attempt to re-classify UCs primarily based on molecular features has revealed that *FGFR3* mutations and overexpression are associated with a subgroup of MIBC with significantly poor prognosis [38]. Although at a

low frequency (3-4%), *FGFR3* and *AKT1* mutations were found to occur together in high-grade UC [43,46]. Overexpression of *FGFR1* is also found in UC across all stages and grades [39]. Further functional studies of FGF and FGFR3 signalling pathway is therefore essential in both NMIBC and MIBC, firstly to allow stratification according to risk of progression and/or recurrence, and secondly to aid in patient selection for potential combination therapies.

Acknowledgements

This work is funded by School of Medicine, College of MVLS, University of Glasgow (TI), Cancer Research UK (OS), and University of Glasgow MRC Centenary Award (MF). We would like to thank Dr Mohammad Derakhshan for his assistance in statistical analysis of TMA results, Iain McPherson, Dionysios Theofilopoulos, Despoina Natsiou, Biological and Histology Services at Beatson Institute for Cancer Research for their technical support.

Author contributions

MF, LK, and TI performed experiments and analysed the results, BWGvR, TvdK, AMB analysed the TMA, RR and OJS advised the mouse cohort design, SF advised on pathology, MF, IA, HYL, and TI wrote the manuscript, OJS and TI supervised the overall project.

References

1. Stenzl A, Cowan NC, De Santis M*, et al.* The updated EAU guidelines on muscle-invasive and metastatic bladder cancer. *Eur Urol* 2009; **55**: 815-825.
2. Zieger K, Dyrskjot L, Wiuf C*, et al.* Role of activating fibroblast growth factor receptor 3 mutations in the development of bladder tumors. *Clin Cancer Res* 2005; **11**: 7709-7719.

3. Herr HW. Tumor progression and survival of patients with high grade, noninvasive papillary (TaG3) bladder tumors: 15-year outcome. *J Urol* 2000; **163**: 60-61; discussion 61-62.
4. Knowles MA. Molecular pathogenesis of bladder cancer. *International Journal of Clinical Oncology* 2008; **13**: 287-297.
5. Billerey C, Chopin D, Aubriot-Lorton MH*, et al.* Frequent FGFR3 mutations in papillary non-invasive bladder (pTa) tumors. *Am J Pathol* 2001; **158**: 1955-1959.
6. Jebar AH, Hurst CD, Tomlinson DC*, et al.* FGFR3 and Ras gene mutations are mutually exclusive genetic events in urothelial cell carcinoma. *Oncogene* 2005; **24**: 5218-5225.
7. Lamy A, Gobet F, Laurent M*, et al.* Molecular profiling of bladder tumors based on the detection of FGFR3 and TP53 mutations. *J Urol* 2006; **176**: 2686-2689.
8. Lindgren D, Liedberg F, Andersson A*, et al.* Molecular characterization of early-stage bladder carcinomas by expression profiles, FGFR3 mutation status, and loss of 9q. *Oncogene* 2006; **25**: 2685-2696.
9. Goetz R, Mohammadi M. Exploring mechanisms of FGF signalling through the lens of structural biology. *Nat Rev Mol Cell Biol* 2013; **14**: 166-180.
10. Laederich MB, Horton WA. FGFR3 targeting strategies for achondroplasia. *Expert Rev Mol Med* 2012; **14**: e11.
11. Iwata T, Chen L, Li C*, et al.* A neonatal lethal mutation in FGFR3 uncouples proliferation and differentiation of growth plate chondrocytes in embryos. *Hum Mol Genet* 2000; **9**: 1603-1613.
12. Iwata T, Li CL, Deng CX*, et al.* Highly activated Fgfr3 with the K644M mutation causes prolonged survival in severe dwarf mice. *Hum Mol Genet* 2001; **10**: 1255-1264.
13. Iwata T, Hevner RF. Fibroblast growth factor signaling in development of the cerebral cortex. *Dev Growth Differ* 2009; **51**: 299-323.

14. Ahmad I, Iwata T, Leung HY. Mechanisms of FGFR-mediated carcinogenesis. *Biochim Biophys Acta* 2012; **1823**: 850-860.
15. Chesi M. Activated fibroblast growth factor receptor 3 is an oncogene that contributes to tumor progression in multiple myeloma. *Blood* 2001; **97**: 729-736.
16. Logie A. Activating mutations of the tyrosine kinase receptor FGFR3 are associated with benign skin tumors in mice and humans. *Human Molecular Genetics* 2005; **14**: 1153-1160.
17. Qing J, Du X, Chen Y*, et al.* Antibody-based targeting of FGFR3 in bladder carcinoma and t(4;14)-positive multiple myeloma in mice. *J Clin Invest* 2009; **119**: 1216-1229.
18. Ahmad I, Singh LB, Foth M*, et al.* K-Ras and {beta}-catenin mutations cooperate with Fgfr3 mutations in mice to promote tumorigenesis in the skin and lung, but not in the bladder. *Dis Model Mech* 2011; **4**: 548-555.
19. Tsuruta H. Hyperplasia and Carcinomas in Pten-Deficient Mice and Reduced PTEN Protein in Human Bladder Cancer Patients. *Cancer Research* 2006; **66**: 8389-8396.
20. Yoo LI, Liu DW, Le Vu S*, et al.* Pten deficiency activates distinct downstream signaling pathways in a tissue-specific manner. *Cancer Res* 2006; **66**: 1929-1939.
21. Ahmad I, Morton JP, Singh LB*, et al.* beta-Catenin activation synergizes with PTEN loss to cause bladder cancer formation. *Oncogene* 2011; **30**: 178-189.
22. Puzio-Kuter AM, Castillo-Martin M, Kinkade CW*, et al.* Inactivation of p53 and Pten promotes invasive bladder cancer. *Genes Dev* 2009; **23**: 675-680.
23. Mo L, Cheng J, Lee EY*, et al.* Gene deletion in urothelium by specific expression of Cre recombinase. *Am J Physiol Renal Physiol* 2005; **289**: F562-568.
24. Lesche R, Groszer M, Gao J*, et al.* Cre/loxP-mediated inactivation of the murinePten tumor suppressor gene. *genesis* 2002; **32**: 148-149.

25. Novak A, Guo C, Yang W*, et al.* Z/EG, a double reporter mouse line that expresses enhanced green fluorescent protein upon Cre-mediated excision. *Genesis* 2000; **28**: 147-155.

26. Dupuy AJ, Rogers LM, Kim J*, et al.* A modified sleeping beauty transposon system that can be used to model a wide variety of human cancers in mice. *Cancer Res* 2009; **69**: 8150-8156.

27. Zhang ZT, Pak J, Shapiro E*, et al.* Urothelium-specific expression of an oncogene in transgenic mice induced the formation of carcinoma in situ and invasive transitional cell carcinoma. *Cancer Res* 1999; **59**: 3512-3517.

28. Kong XT. Roles of uroplakins in plaque formation, umbrella cell enlargement, and urinary tract diseases. *The Journal of Cell Biology* 2004; **167**: 1195-1204.

29. Shin K, Lee J, Guo N*, et al.* Hedgehog/Wnt feedback supports regenerative proliferation of epithelial stem cells in bladder. *Nature* 2011; **472**: 110-114.

30. Castillo-Martin M, Domingo-Domenech J, Karni-Schmidt O*, et al.* Molecular pathways of urothelial development and bladder tumorigenesis. *Urologic Oncology: Seminars and Original Investigations* 2010; **28**: 401-408.

31. Lopez-Knowles E, Hernandez S, Malats N*, et al.* PIK3CA mutations are an early genetic alteration associated with FGFR3 mutations in superficial papillary bladder tumors. *Cancer Res* 2006; **66**: 7401-7404.

32. van Rhijn BW, Montironi R, Zwarthoff EC*, et al.* Frequent FGFR3 mutations in urothelial papilloma. *J Pathol* 2002; **198**: 245-251.

33. Ross RL, Askham JM, Knowles MA. PIK3CA mutation spectrum in urothelial carcinoma reflects cell context-dependent signaling and phenotypic outputs. *Oncogene* 2013; **32**: 768-776.

34. Brooks AN, Kilgour E, Smith PD. Molecular pathways: fibroblast growth factor signaling: a new therapeutic opportunity in cancer. *Clin Cancer Res* 2012; **18**: 1855-1862.

35. Lamont FR, Tomlinson DC, Cooper PA*, et al.* Small molecule FGF receptor inhibitors block FGFR-dependent urothelial carcinoma growth in vitro and in vivo. *Br J Cancer* 2011; **104**: 75-82.

36. Guagnano V, Furet P, Spanka C*, et al.* Discovery of 3-(2,6-dichloro-3,5-dimethoxy-phenyl)-1-{6-[4-(4-ethyl-piperazin-1-yl)-phenylamin o]-pyrimidin-4-yl}-1-methyl-urea (NVP-BGJ398), a potent and selective inhibitor of the fibroblast growth factor receptor family of receptor tyrosine kinase. *J Med Chem* 2011; **54**: 7066-7083.

37. Gavine PR, Mooney L, Kilgour E*, et al.* AZD4547: an orally bioavailable, potent, and selective inhibitor of the fibroblast growth factor receptor tyrosine kinase family. *Cancer Res* 2012; **72**: 2045-2056.

38. Sjodahl G, Lauss M, Lovgren K*, et al.* A molecular taxonomy for urothelial carcinoma. *Clin Cancer Res* 2012; **18**: 3377-3386.

39. Tomlinson DC, Lamont FR, Shnyder SD*, et al.* Fibroblast growth factor receptor 1 promotes proliferation and survival via activation of the mitogen-activated protein kinase pathway in bladder cancer. *Cancer Res* 2009; **69**: 4613-4620.

40. Cho JY, Guo C, Torello M, et al. Defective lysosomal targeting of activated fibroblast growth factor receptor 3 in achondroplasia. *Proc Natl Acad Sci U S A* 2004; **101**: 609-614.

41. Platt FM, Hurst CD, Taylor CF, et al. Spectrum of phosphatidylinositol 3-kinase pathway gene alterations in bladder cancer. *Clin Cancer Res* 2009; **15**: 6008-6017.

42. Kompier LC, Lurkin I, van der Aa MN, et al. FGFR3, HRAS, KRAS, NRAS and PIK3CA mutations in bladder cancer and their potential as biomarkers for surveillance and therapy. *PLoS One* 2010; **5**: e13821.

43. Juanpere N, Agell L, Lorenzo M, et al. Mutations in FGFR3 and PIK3CA, singly or combined with RAS and AKT1, are associated with AKT but not with MAPK pathway activation in urothelial bladder cancer. *Hum Pathol* 2012; **43**: 1573-1582.

44. Duenas M, Martinez-Fernandez M, Garcia-Escudero R, et al. PIK3CA gene alterations in bladder cancer are frequent and associate with reduced recurrence in non-muscle invasive tumors. *Mol Carcinog* 2013. doi: 10.1002/mc.22125.

45. Calderaro J, Rebouissou S, de Koning L, et al. PI3K/AKT pathway activation in bladder carcinogenesis. *Int J Cancer* 2013. doi: 10.1002/ijc.28518.

46. Askham JM, Platt F, Chambers PA, et al. AKT1 mutations in bladder cancer: identification of a novel oncogenic mutation that can co-operate with E17K. *Oncogene* 2010; **29**: 150-155.

47. Korkolopoulou P, Levidou G, Trigka EA, et al. A comprehensive immunohistochemical and molecular approach to the PI3K/AKT/mTOR (phosphoinositide 3-kinase/v-akt murine thymoma viral oncogene/mammalian target of rapamycin) pathway in bladder urothelial carcinoma. *BJU Int* 2012; **110**: E1237-1248.

48. Yohn NL, Bingaman CN, DuMont AL, et al. Phosphatidylinositol 3'-kinase, mTOR, and glycogen synthase kinase-3beta mediated regulation of p21 in human urothelial carcinoma cells. *BMC Urol* 2011; **11**: 19.

49. Tomlinson DC, Blado O, Hamden P, *et al.* FGFR3 protein expression and its relationship to mutation status and prognostic variables in bladder cancer. *J Pathol* 2007; **213**: 91-98.

Table 1: Summary of mouse cohorts and bladder phenotype

Genotype	Cohort size (n)	Age at time of analysis	Non-bladder related deaths (n)	Increased urothelial thickness (n)	Cellular abnormalities (n)
Control	11	10-18 months	None	None	None
UroIICre *Fgfr3*$^{+/K644E}$	25	5-15 months	2 (8%)	None	None
UroIICre *Pten*$^{flox/flox}$	20	9-18 months	4 (20%)	12 (60%) mild	None
UroIICre *Fgfr3*$^{+/K644E}$ *Pten*$^{flox/flox}$	24	11-18 months	4 (17%)	4 (17%) mild, 19 (79%) severe, 23 (96%) total	20 (83%)
UroIICre *Fgfr3*$^{K644E/K644E}$	12	7-13 month	10 (83%)*	11 (92%) mild	None
UroIICre *Fgfr3*$^{K644E/K644E}$ *Pten*$^{flox/flox}$	3	10-12 months	None	2 (66%) severe	2 (66%)

The mouse cohorts analysed in this study are summarised. Cellular abnormalities observed include vacuolisation, enlarged cells, and loss of cell orientation within the urothelium. Causes of non-bladder related deaths include infection and lymphoma, and termination due to skin rash on the back owing to Cre-lox recombination occurred in the epidermis [18]. **UroIICreFgfr3*$^{K644E/K644E}$ mice were sacrificed at the time when kyphosis became prevalent. This phenotype is due to a low-level of Fgfr3 expression in the presence of homozygous *Fgfr3*^{K644Eneo} allele [11].

Figure legends

Figure 1: Increased thickness of the *UroIICreFgfr3*$^{+/K644E}$*Pten*$^{flox/flox}$ urothelium. Representative images of H&E stained bladder sections of *Control* (a, e), *UroIICreFgfr3*$^{+/K644E}$ (b, f), *UroIICrePten*$^{flox/flox}$ (c, g) and *UroIICreFgfr3*$^{+/K644E}$ *Pten*$^{flox/flox}$ (d, h) at low (a-d) and high magnification (e-h). The murine urothelium consists of three layers, namely umbrella, intermediate, and basal cells and borders with connective tissue and the stroma (e, *insert*). Scale bar represents 200 µm in panel a-d and 100 µm in panel e-h. Thickness of the urothelium was quantified in *Control, UroIICreFgfr3*$^{+/K644E}$ (Fgfr3), *UroIICrePten*$^{flox/flox}$ (Pten) and *UroIICreFgfr3*$^{+/K644E}$*Pten*$^{flox/flox}$ (Fgfr3Pten) in the number of animals indicated (i). The error bars indicate the standard deviations.

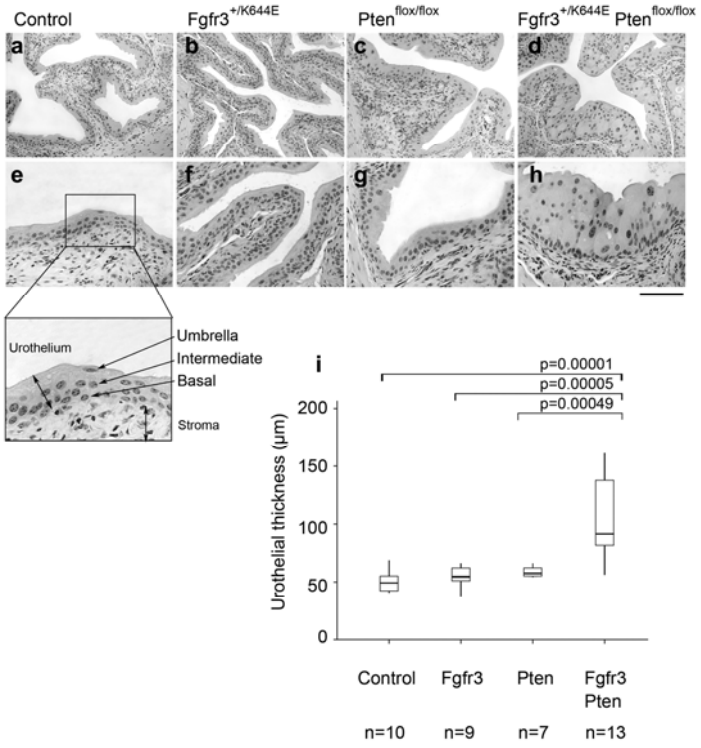

Figure 2: Abnormal cellular morphology in the *UroIICreFgfr3*$^{+/K644E}$*Pten*$^{flox/flox}$ urothelium. A, Representative images of H&E-stained *Control* (a, d) and *UroIICreFgfr3*$^{+/K644E}$*Pten*$^{flox/flox}$ urothelia (b, c, e, f) at low (a-c) and high magnification (d-f). Vacuolisation (arrow in c), condensed cellular appearance (circled in e), enlargement of cells and nuclei (arrow heads in e, f), and loss of polarity were observed. Periodic acid-Schiff (PAS) staining marked glycogen-rich vacuoles in *UroIICreFgfr3*$^{+/K644E}$*Pten*$^{flox/flox}$ (g). **B,** Expression of UroplakinII (a, e, i), CK5 (b, f, j and d, h, l), p63 (c, g, k), CK18 (d, h, l) was used to assess differentiation of umbrella (UroII and CK18), intermediate (p63) and basal cells (p63 and CK5) in *Control* (a-d) and *UroIICreFgfr3*$^{+/K644E}$*Pten*$^{flox/flox}$ (e-l) (immunohistochemistry). Double staining with CK18 (green) and CK5 (red) (d, h, l) shows the abnormal localisation of CK18-positive cells deeper in the urothelium of *UroIICreFgfr3*$^{+/K644E}$*Pten*$^{flox/flox}$. Scale bar represents 200 µm in A (a-c) and 100 µm in A (d-g), B (a-l).

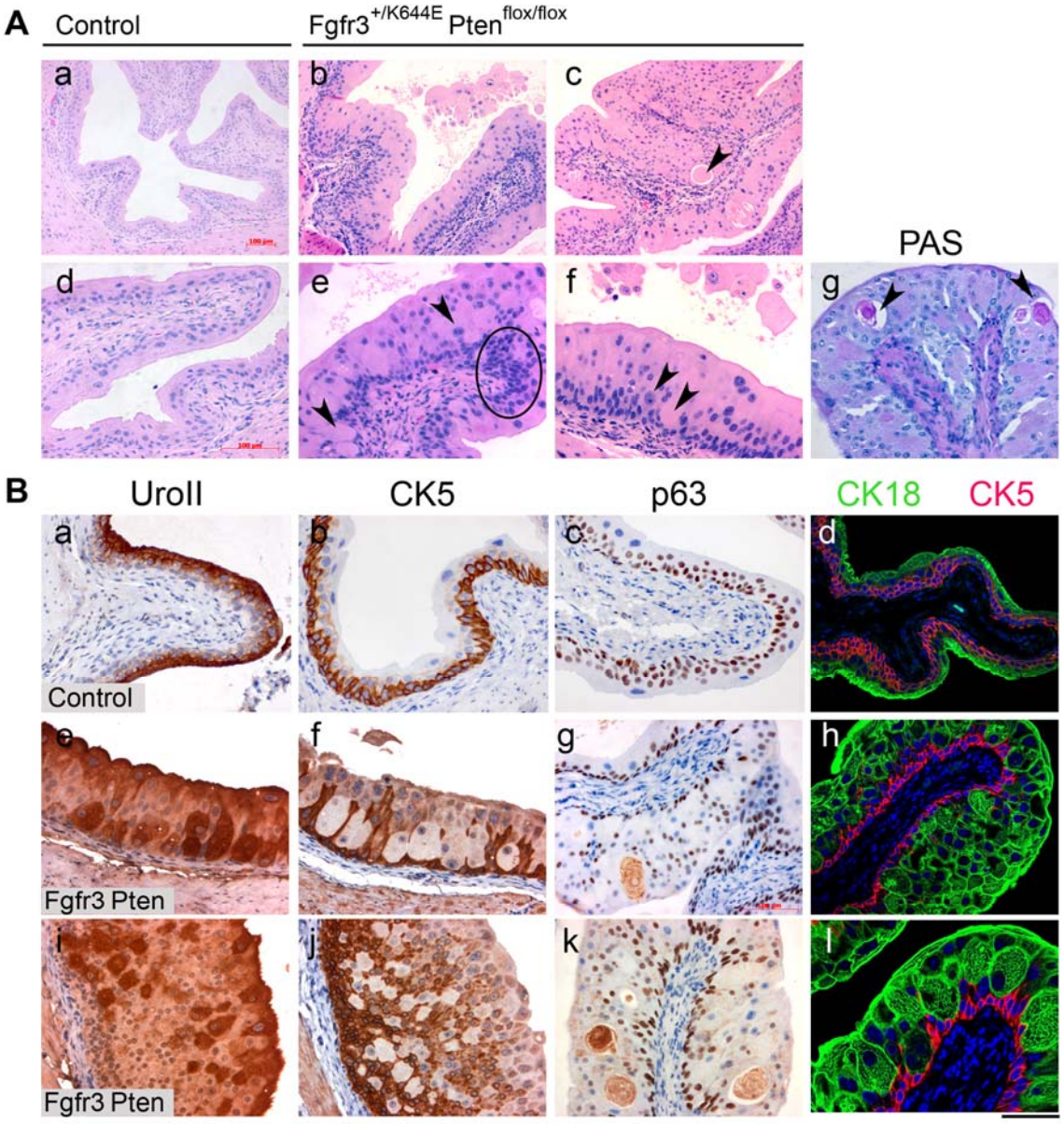

Figure 3: Differential effects of *Fgfr3* and *Pten* mutations in regulation of urothelial cell size and proliferation. The cell size of was analysed comparing cells in each layer using immunohistochemistry with E-cadherin. The sizes of cells in the outermost umbrella (a) and innermost basal (c) cell layers did not show any significant differences among the cohorts. However increase in cell size was observed in the intermediate (between the inner and outmost) layer, in particular in *UroIICrePten*$^{flox/flox}$ and in *UroIICre Fgfr3*$^{+/K644E}$*Pten*$^{flox/flox}$ (b). Ki67-positive cells were increased in the urothelium of *UroIICrePten*$^{flox/flox}$ as well as *UroIICreFgfr3*$^{+/K644E}$*Pten*$^{flox/flox}$ mice, comparing to other cohorts (d). The error bars indicate the standard deviations.

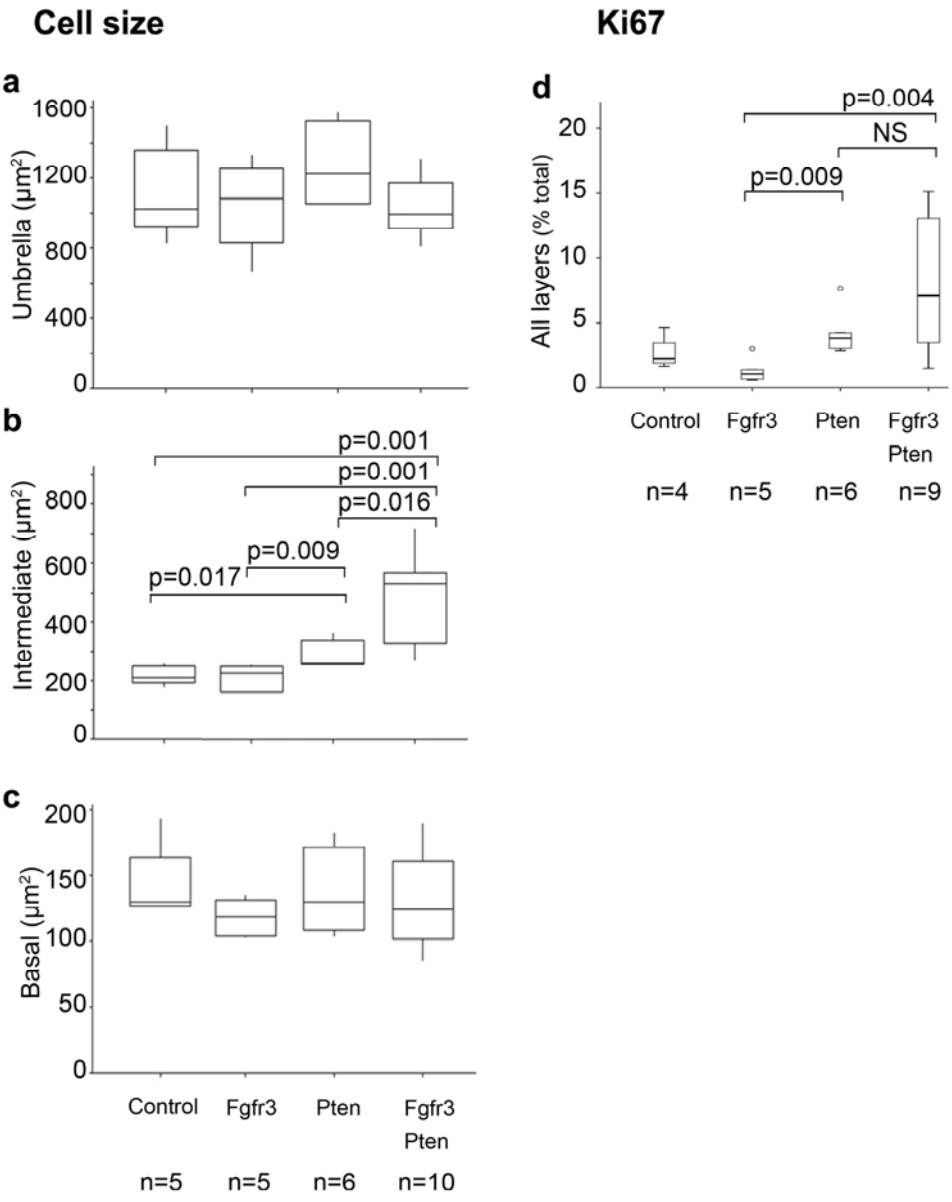

Figure 4: **Deregulation of downstream signalling and cell cycle arrest in the *UroIICreFgfr3$^{+/K644E}$Pten$^{flox/flox}$* urothelium.** Immunohistochemistry was performed in *Control* (a-c), *UroIICreFgfr3$^{+/K644E}$* (d-f), *UroIICrePten$^{flox/flox}$* (g-i), and *UroIICreFgfr3$^{+/K644E}$Pten$^{flox/flox}$* urothelia (j-l) with antibodies against phosphorylated Erk1/2 (pErk) (a, d, g, j), phosphorylated Akt (pAkt) (b, e, h, k) and p21 (c, f, i, l). (m) Levels of FGFR3 expression and p-mTOR were semi-quantitatively evaluated in TMA containing T1 urothelial tumours using the 4-point scale (negative, faint, intermediate, strong). Scale bar represents 50 µm in a, b, d, e, g, h, j, k, 100 µm in c, f, i, l, 25 µm in inserts of j-k and 50 µm in insert l.